Non-Arrhenius relaxation effects in collections of two-level subsystems

R. M. Roshko and C. A. Viddal
Department of Physics and Astronomy, University of Manitoba, Winnipeg, Manitoba R3T 2N2, Canada
(Received 11 August 2005; published 18 November 2005)

We present numerical simulations of relaxation isotherms for an ensemble of thermally activated, two-level subsystems, with double-well free energy profiles, and with a distribution of dissipation barriers and level splittings. The field history imitates a typical experimental viscosity protocol, and consists of saturation in a large positive field, followed by recoil to a negative holding field, and then by the thermally driven decay of the moment towards equilibrium at fixed temperature and fixed field. The numerical simulations show that systems whose relaxation dynamics are governed explicitly by the Arrhenius law of thermal activation, can exhibit relaxation effects which are apparently "non-Arrhenius" in origin. In particular, the maximum value of the relaxation rate $S \equiv -\partial M(t)/\partial \ln t$ extracted from model viscosity isotherms over a typical experimental time window 100 s $\leqslant t \leqslant 10^4$ s, and the thermal viscosity field $\hat{H}_f(T)$ extracted, over the same time window, from the field dependence of the logarithm of the time at which the moment reverses direction as it relaxes towards equilibrium, both exhibit variations with temperature which are highly nonlinear, and which are characterized by coincident maxima, very similar to those observed experimentally in a variety of particulate systems.

DOI: 10.1103/PhysRevB.72.184422 PACS number(s): 75.60.−d, 75.75.+a

I. INTRODUCTION

A material is said to exhibit hysteresis[1] if its physical response to an imposed excitation at time t is not determined uniquely by the instantaneous value of the excitation, but instead depends upon its previous history of exposure to the excitation at earlier times $t' \leqslant t$. From a fundamental perspective, hysteresis requires the existence of multiple local minima in the free energy hypersurface of the material in some appropriate multidimensional configuration space.[1] These minima trap the system temporarily in metastable configurations during the course of its migration through configuration space, and prevent it from reaching true thermodynamic equilibrium within the time scale of the experiment. Transitions between metastable states are induced jointly by changes in the excitation field, which distort the free energy landscape and convert local minima to saddle points, and by thermal overbarrier fluctuations, which drive the system towards thermal equilibrium. Since the time required to surmount an energy barrier W at temperature T is $\tau = \tau_0 \exp(W/kT)$, where τ_0 is a characteristic microscopic time (typically assumed to be between 10^{-12} s and 10^{-9} s), thermal fluctuations introduce a dependence on observation time t into the system response functions.

In magnetic materials, the relaxation of the magnetic properties that accompanies the spontaneous approach to equilibrium is of considerable interest, both for fundamental reasons, as well as for the practical limitations that it imposes on the ultimate bit size of information storage media and on the stability of permanent magnets. Attention is focused primarily on the relaxation of the magnetic moment $M(t)$, and on the field and temperature dependence of the relaxation rate $S \equiv -\partial M(t)/\partial \ln t$. Magnetic viscosity experiments performed on particulate media, with particle dimensions ranging from microns to nanometers, which measure the decay of the moment after recoiling from positive saturation to negative holding fields $-H_a$ in the vicinity of the measured coercive field H_c, yield a temperature dependent relaxation rate S with a well-defined maximum,[2,3] and various analytical techniques[4,5] designed to extract from these viscosity measurements the *thermal fluctuation field* $H_f = kT/\mu$, a concept first introduced by Néel[6] in order to quantify the effects of thermal fluctuations in terms of an effective activation moment reversal, μ, yield similar maxima in the temperature dependence of H_f.[3,7] This behavior is referred to in the literature as "non-Arrhenius," and it has recently been suggested that its physical origins may lie in a Bose-Einstein condensation of magnons.[7,8]

The theoretical foundation for the various analytical techniques mentioned above is the Preisach model of hysteresis.[9] In this paper, we review the essential arguments on which these techniques are based, and we show that the Preisach formalism, which is based explicitly on an Arrhenius picture of thermal activation, is nevertheless capable of yielding non-Arrhenius behavior when experimental measurements are restricted to a single limited temporal observation window.

II. THE MODEL

The representation of magnetic materials as collections of elementary bistable subsystems was first introduced into the literature by Preisach,[9] and has since evolved into a formal theoretical framework for the unified description of hysteresis and thermal relaxation, based on simple free energy considerations that are fundamental to all history-dependent phenomena.[5,10–12] The model is based on the postulate that the free energy hypersurface of the material can be decomposed into an ensemble of one-dimensional fragments, each with a double well free energy profile in a two-state configuration space,[1] as shown in Fig. 1. The subsystems represent the Barkhausen instabilities, which are fundamental to all magnetizing processes and are characterized individually by a magnetic moment μ, two magnetic configurations $\pm\mu$, a

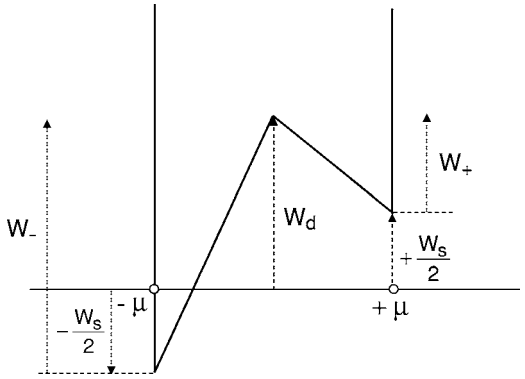

FIG. 1. The double well free energy profile of a single Preisach subsystem with moment μ, states $\pm\mu$, dissipation barrier $W_d = \mu H_d$, level splitting $W_s = 2\mu H_s$, and excitation energies W_+ and W_-.

dissipation barrier $W_d = \mu H_d$, which describes the energy lost irreversibly as heat in a Barkhausen transition, a free energy difference $W_s = 2\mu H_s$ between the two states, and two excitation barriers to moment reversal, $W_+ = \mu(H_d - H_s) = -\mu H_+$ and $W_- = \mu(H_d + H_s) = \mu H_-$, and collectively by a distribution $p(H_d, H_s)$ of characteristic fields H_d and H_s. Transitions are activated by a combination of an external magnetic field H_a and an effective thermal viscosity field[10] $H_T = H_f \ln(t/\tau_0)$, where $H_f = kT/\mu$ is the thermal fluctuation field, t is the experimental time constant, and τ_0 is a microscopic time that is typically assumed to be between 10^{-12} s and 10^{-9} s. When the thermal viscosity field H_T exceeds the lower of the two excitation fields of a given subsystem (H_d, H_s), that is, when $H_T > H_{lower} = H_d - |H_a - H_s|$, then the subsystem is considered to be in thermal equilibrium, and its moment is given by $m_{eq} = \mu \tanh[\mu(H_a - H_s)/kT]$. The excitation barriers (W_+, W_-) and the equivalent fields (H_d, H_s) are to be regarded as *intrinsic* characteristics of the material at any given temperature which, in principle, would define the magnetic response of the material in the hypothetical limit where all changes in field and temperature could be accomplished *instantaneously*.[5] The total moment of the ensemble is a history-dependent superposition of the individual subsystem moments, weighted by the Preisach density:

$$M(H_a,T) = N \int_0^{\infty} dH_d \int_{-\infty}^{+\infty} dH_s m(H_d, H_s, \text{history of } H_a, T, t) \times p(H_d, H_s, T), \quad (1)$$

where N is the total number of subsystems, and $m = +\mu(T)$, or $m = -\mu(T)$, or, $m = m_{eq} = \mu(T)\tanh[\mu(T)(H_a - H_s)/kT]$, depending upon the history of field applications and reversals and the experimental observation time t.

Although the various Preisach-based prescriptions that have been developed for analyzing magnetic viscosity measurements[4,5] differ somewhat in specific details, the physical arguments are fundamentally the same and can be paraphrased as follows. The relaxation of the magnetic moment observed in negative holding fields $-H_a$ (with $H_a > 0$) is due to those Preisach subsystems with $-H_a < H_s < H_d - H_a$ which are trapped in their higher energy metastable state $m = +\mu$, with excitation barrier $W'_+ = \mu(H_d - H_s - H_a)$, after recoil from positive saturation. These subsystems will be thermally activated and will relax to their superparamagnetic equilibrium configuration $m = -\mu \tanh[\mu(H_s + |H_a|)/kT] \cong -\mu$ at a time $t = t_c$ when

$$H_T = (kT/\mu)\ln(t_c/\tau_0) = W'_+/\mu = H_d - H_s - H_a, \quad (2)$$

that is, when

$$\ln t_c = -(\mu/kT)H_a + [(\mu/kT)(H_d - H_s) + \ln \tau_0], \quad (3)$$

so that, for a given subsystem (H_d, H_s), $\ln t_c$ is predicted to vary *linearly* with H_a, with a slope that is inversely proportional to the thermal fluctuation field H_f, and with an intercept that contains the intrinsic excitation barrier $H_d - H_s$ for that subsystem. Of course, measured relaxation isotherms are actually a superposition of relaxation events involving the

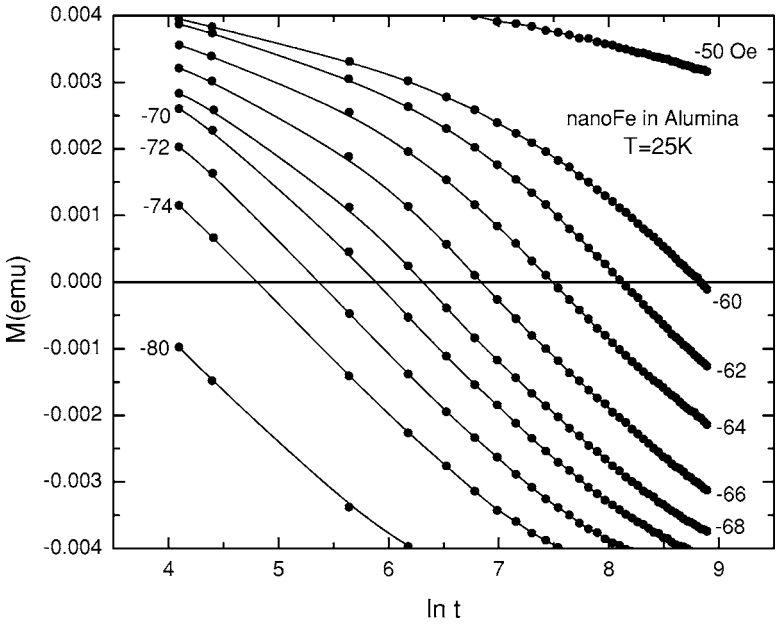

FIG. 2. Viscosity isotherms measured in a series of negative holding fields at a temperature $T = 25$ K and plotted as a function of lnt for a thin film of Fe nanoparticles embedded in alumina. The numbers next to the isotherms are the holding fields $-H_a$ in Oe.

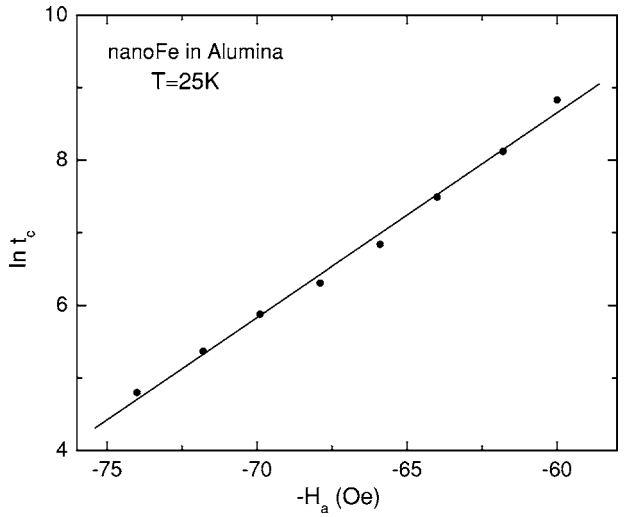

FIG. 3. A plot of $\ln t_c$, where t_c is the time at which a given viscosity isotherm in Fig. 2 reverses sign, as a function of holding field $-H_a$ at $T=25$ K.

entire spectrum of Preisach subsystems, each with its own characteristic relaxation time t_c, and the value of $\ln t_c$ for the *system* must be determined by performing the integral in Eq. (1). Nevertheless, plots of $\ln t_c$ versus H_a obtained from viscosity isotherms measured on a variety of particulate media are indeed linear within experimental uncertainty, and the slope of these plots yields a thermal fluctuation field H_f with a highly nonlinear temperature dependence, and with a well-defined maximum. Figures 2, 3, and 4 illustrate a typical analysis performed on a thin film of Fe nanoparticles embedded in alumina. Figure 2 shows a set of viscosity isotherms measured at $T=25$ K in a series of negative holding fields and plotted as a function of $\ln t$, Fig. 3 shows the plot of $\ln t_c$ versus H_a for $T=25$ K, where t_c is the time at which the moment reverses sign, and Fig. 4 shows the temperature dependence of the inverse slope H_f and of the intercept H_{int} along the field axis at $t=\tau_0$, assuming $\tau_0=10^{-9}$ s. Similar results are obtained from related approaches, which collapse the viscosity isotherms for different holding fields at a given temperature onto universal curves using appropriately defined scaling variables. It is the nonlinear behavior of H_f in Fig. 4 which is described as "non-Arrhenius" in the literature, and which has been attributed to magnon condensation.[7,8]

III. NUMERICAL SIMULATIONS

In order to further explore the origins of this nonlinear behavior, we have generated numerical simulations of viscosity isotherms using the Preisach formalism, and assuming a Preisach characteristic field density consisting of the product of a lognormal distribution of dissipation fields H_d and a Gaussian distribution of bias fields H_s:

$$p(H_d,H_s)=(2\pi\sigma_d^2H_d^2)^{-1/2}\exp[-[\ln(H_d/\bar{H}_d)]^2/2\sigma_d^2]\times(2\pi\sigma_s^2)^{-1/2}\exp(-H_s^2/2\sigma_s^2). \quad (4)$$

Figure 5 shows the magnetic states of all of the subsystems at a time t after recoiling from positive saturation to a negative holding field $-H_a$ at a temperature T. Each subsystem is identified by its characteristic field coordinates with respect to orthogonal (H_d,H_s) axes, or equivalently orthogonal (H_-,H_+) axes. The integral in Eq. (1) extends over the entire triangular area in Fig. 5, which defines the limits of the distribution in Eq. (4). The numerical simulations are summarized in Figs. 6, 7, and 8 for a Preisach density with parameters $\bar{H}_d=100$ Oe, $\sigma_d=0.5$, and $\sigma_s=50$ Oe, and assuming a temperature independent subsystem saturation moment $\mu=3\times10^{-15}$ emu.

Figure 6 shows numerical relaxation isotherms generated for a series of negative holding fields $-H_a$ between 0 and -106 Oe, and plotted as a function of the variable $(kT/\mu)\ln(t/\tau_0)$, which is just the thermal viscosity field H_T. Since the only source of temperature dependence in the model other than H_T is the comparatively weak dependence

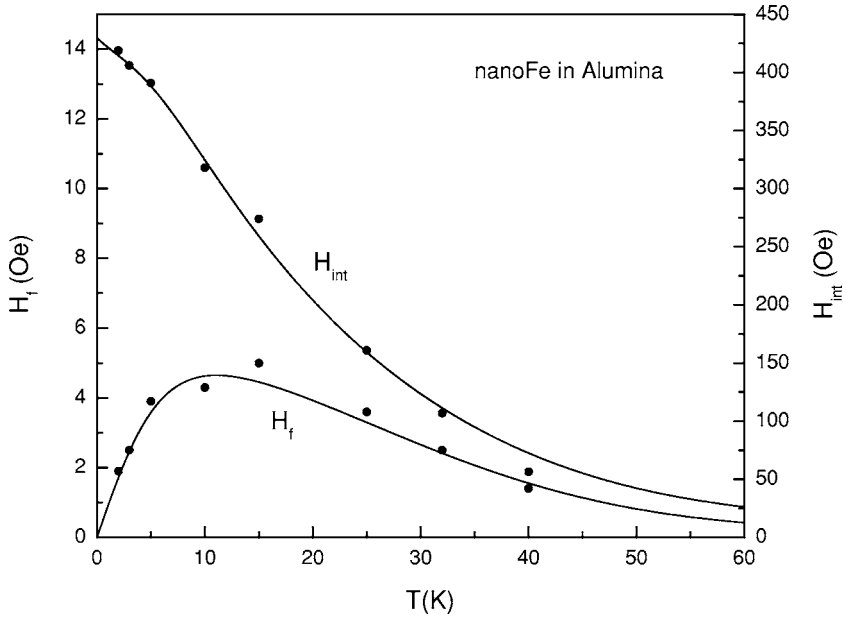

FIG. 4. The temperature dependence of the inverse slope H_f and of the intercept H_{int} obtained from plots of $\ln t_c$ versus $-H_a$ like that shown in Fig. 3. The solid curves are guides to the eye.

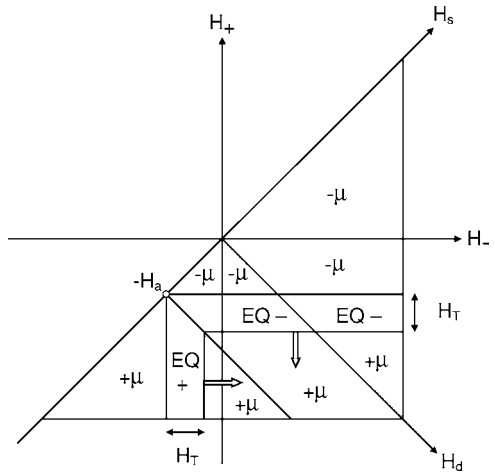

FIG. 5. The Preisach plane showing the configuration of all of the subsystems in the presence of a negative holding field $-H_a$ and a thermal viscosity field $H_T=(kT/\mu)\ln(t/\tau_0)$. The portions of the plane labeled EQ+ and EQ– identify those subsystems which are in thermal equilibrium, and hence which respond superparamagnetically. The open arrows show the effect of increasing observation time on the Preisach boundaries.

associated with the equilibrium subsystem moment $m_{eq}=\mu(T)\tanh[\mu(T)(H_a-H_s)/kT]$, such plots produce *universal curves* for each holding field, valid for all temperatures T, and all observation times t. The vertical lines in Fig. 6 illustrate how changes in temperature have the effect of selecting different portions of these universal curves, for a typical fixed observation window $100\ \mathrm{s}\leqslant t\leqslant 10^4$ s. Figure 7 shows a plot of $(kT/\mu)\ln(t_c/\tau_0)$, where t_c is the time at which the relaxation isotherm for a particular holding field in Fig. 6 reverses sign, as a function of holding field $-H_a$. This curve is also universal, in the sense that it is valid for all temperatures and all observation times, and the horizontal lines in this figure illustrate the portions of this curve that would be selected in an experiment performed at different temperatures, but over a fixed observation time window $100\ \mathrm{s}\leqslant t\leqslant 10^4$ s. If we adopt a linear approximation for each of these segments, in order to imitate experimental data like those in Fig. 3, so that

$$(kT/\mu)\ln(t_c/\tau_0)\cong -\alpha H_a+\beta, \tag{5}$$

then it follows that

$$\ln(t_c/\tau_0)\cong -(\alpha/H_f)H_a+\beta/H_f, \tag{6}$$

and hence that a plot of $\ln(t_c/\tau_0)$ versus $-H_a$ will depend on the local slope α of that portion of the universal curve that is selected by the particular experimental temperature. For low values of $(kT/\mu)\ln(t_c/\tau_0)$, the universal curve is exactly linear and its local slope is exactly $\alpha=1$, so that the slope of Eq. (6) will yield the true value of H_f. However, where the universal curve departs from linearity, Eq. (6) will yield a "fictitious" thermal fluctuation field $\hat{H}_f\equiv H_f/\alpha$ which depends on α, a parameter that is not known *a priori*. Figure 8 shows a plot of the temperature dependence of the "fictitious" fluctuation field $\hat{H}_f$ determined in this way from the numerical data in Fig. 7. The fictitious field is identical to the true fluctuation field (straight line in Fig. 8) only at the lowest measurement temperatures, but exhibits progressively more severe departures from H_f as the temperature increases, and eventually passes through a maximum just like that observed experimentally. Figure 8 also shows the temperature dependence of the intercept $\hat{\beta}$ of Eq. (6) with the H_a-axis at $t_c=\tau_0$. At low temperatures, this intercept is constant and is identical to the intrinsic coercive field $H_c(0)$ characteristic of this particular distribution, in the limit $H_T=0$. However, with increasing temperature, the intercept exhibits systematic deviations from $H_c(0)$, which are clearly correlated with the deviations from linearity observed in $\hat{H}_f$, and which indicate that the intercept is *not* a reliable probe of the *intrinsic* free

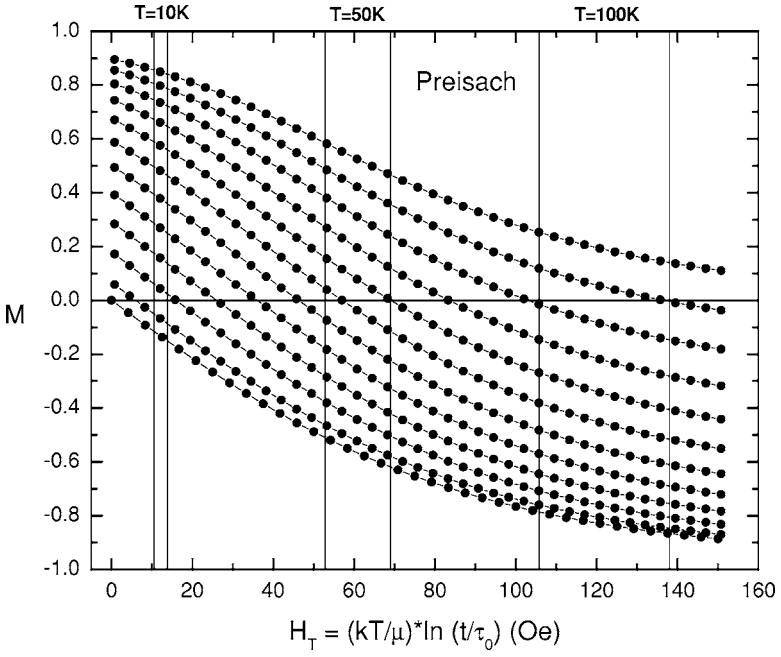

FIG. 6. Preisach model simulations of universal relaxation isotherms plotted as a function of $H_T=(kT/\mu)\ln(t/\tau_0)$ for a series of negative holding fields $-H_a=0,-10,-20,-30,-40,-50,-60,-70,-80,-90$, and -106 Oe (top to bottom). The vertical lines show the segments of the isotherms that would be visible in an experiment performed over a fixed observation time window $100\ \mathrm{s}\leqslant t\leqslant 10^4$ s at several representative temperatures $T=10$, 50, and 100 K.

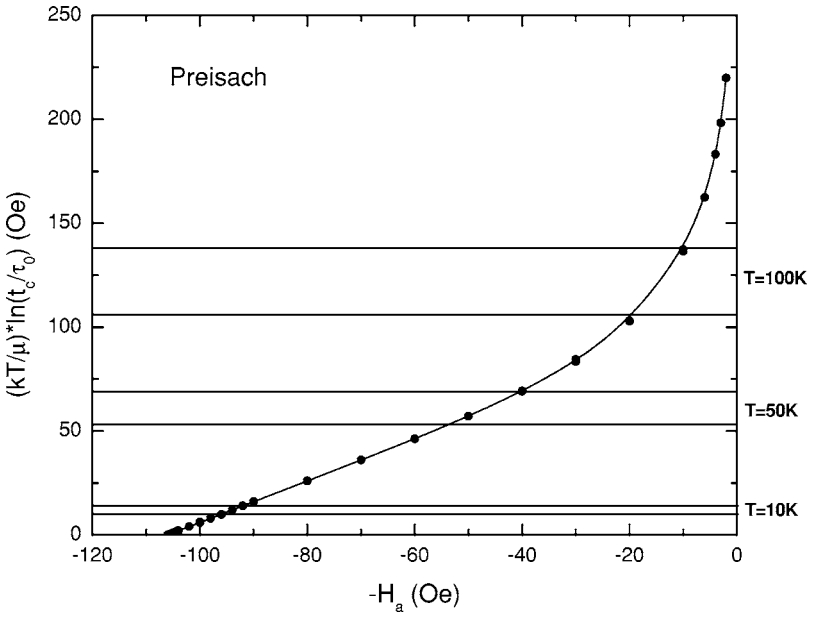

FIG. 7. A universal curve generated by plotting $(kT/\mu)\ln(t_c/\tau_0)$ for the numerical relaxation isotherms in Fig. 6 as a function of $-H_a$. The horizontal lines show the portions of the universal curve that would be sampled in an experiment performed over a fixed observation time window $100\ \mathrm{s} \leqslant t \leqslant 10^4\ \mathrm{s}$ at several different temperatures $T=10$, 50, and 100 K.

energy landscape which, in the current scenario, is independent of temperature.

The temperature dependences $\hat{H}_f(T)$ and $\hat{\beta}(T)$ in Fig. 8 are a function of the characteristics of the Preisach distribution and of the subsystem moment. Decreases (increases) in μ shift the deviations to lower (higher) temperatures. If one of the two distribution functions is very narrow (either $\sigma_d \ll \bar{H}_d$ or $\sigma_s \ll \bar{H}_d$), then the universal curve in Fig. 7 is linear over a wider range of holding fields, and the deviations in $\hat{H}_f(T)$ and $\hat{\beta}(T)$ are delayed to higher temperatures.

Finally, we point out that the maximum in $\hat{H}_f(T)$ is accompanied by a maximum in the temperature dependence of the relaxation rate $S \equiv -\partial M(t)/\partial \ln t$ which, in terms of the universal relaxation functions $M(t)=f_{Ha}[H_T=(kT/\mu)\ln(t/\tau_0)]$ in Fig. 6, is given by

$$S = -(\partial f_{Ha}(H_T)/\partial H_T)(\partial H_T/\partial \ln t) = -(kT/\mu)(\partial f_{Ha}(H_T)/\partial H_T). \tag{7}$$

For each viscosity field (H_T) window in Fig. 6, defined by a fixed observation time interval $100\ \mathrm{s} \leqslant t \leqslant 10^4\ \mathrm{s}$ and by a particular temperature T, a typical relaxation isotherm, which reverses sign in the middle of the window, was chosen and differentiated, and the maximum value of $\hat{S} \equiv -\partial f_{Ha}(H_T)/\partial H_T$ was substituted into Eq. (7). Even allowing for the obvious uncertainty in $\hat{S}$ associated with the specific choice of the representative isotherm in a given H_T window, this procedure yields a definite maximum in the temperature dependence of $S(T)$, as shown in Fig. 9, which resembles that observed experimentally,[2,3] and which is coincident with the maximum in $\hat{H}_f(T)$.

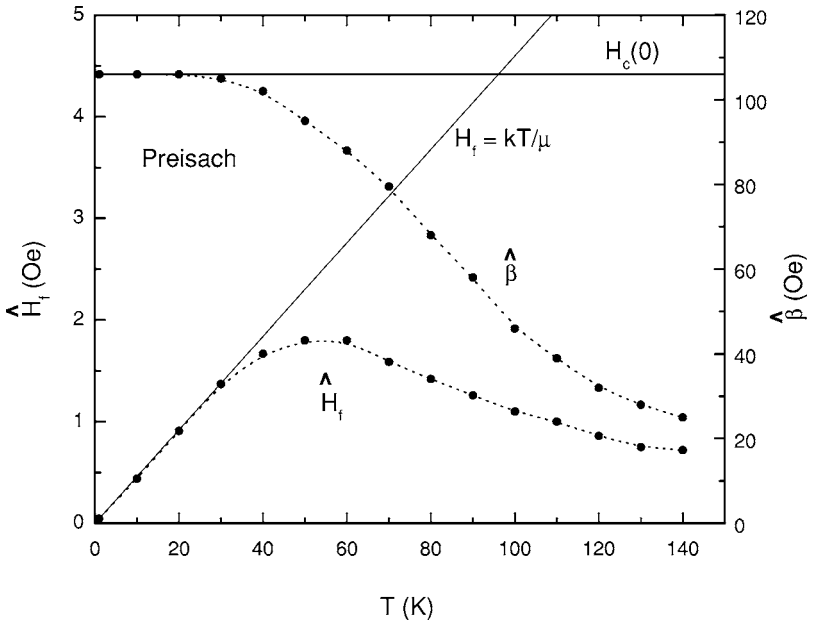

FIG. 8. A plot of the inverse slope $\hat{H}_f(T)$ and of the intercept $\hat{\beta}(T)$ obtained by adopting a linear approximation for each segment of the universal curve in Fig. 7, which is selected by the fixed experimental time window $100\ \mathrm{s} \leqslant t \leqslant 10^4\ \mathrm{s}$ and by a particular measurement temperature T.

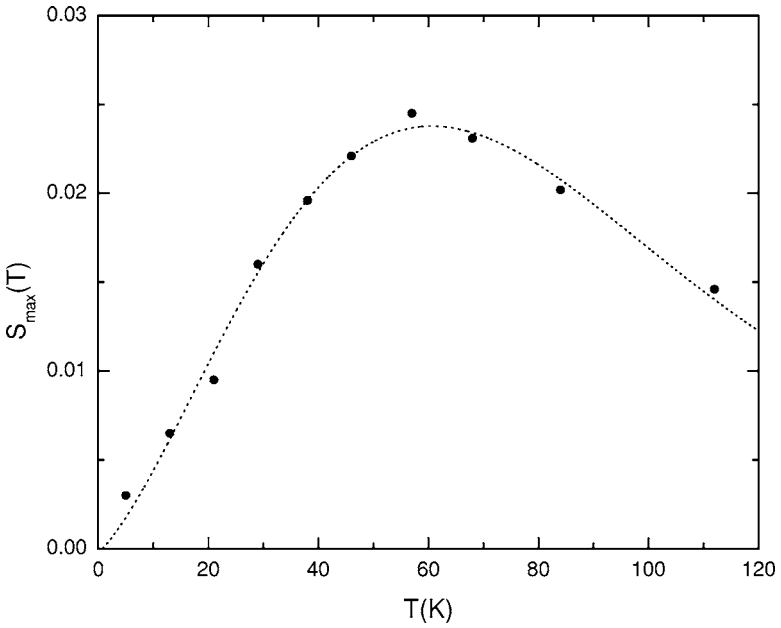

FIG. 9. A plot of the temperature dependence of the maximum relaxation rate $S \equiv -\partial M(t)/\partial \ln t$ obtained from the numerical relaxation isotherms in Fig. 6, assuming a fixed experimental time window $100\ \mathrm{s} \leqslant t \leqslant 10^4\ \mathrm{s}$.

IV. DISCUSSION

The model calculations presented above demonstrate clearly that collections of two-level subsystems whose relaxation dynamics are governed explicitly by the Arrhenius law of thermal activation can exhibit effects which are apparently non-Arrhenius in origin. In particular, the maximum relaxation rate $S(T)$ extracted from viscosity isotherms over a typical experimental time window $100\ \mathrm{s} \leqslant t \leqslant 10^4\ \mathrm{s}$, and the thermal viscosity field $\hat{H}_\mathrm{f}(T)$ extracted, over the same time window, from the field dependence of the logarithm of the time at which the moment reverses direction, both exhibit variations with temperature that are highly nonlinear, and that are characterized by coincident maxima.

The origin of the curvature in the universal function in Fig. 7, which is ultimately the source of the maximum in the temperature dependence of the thermal fluctuation field $\hat{H}_\mathrm{f}$, is easy to appreciate from an inspection of the Preisach diagram in Fig. 10. The horizontal line in this figure, which intersects the H_s axis at $-H_\mathrm{c}(0)$, shows the location of the *intrinsic* coercive field $H_\mathrm{c}(0)$, which reduces the total moment to zero in the limit $H_\mathrm{T}=0$. The integrated moment of the subsystems above this line, all of which are in their $-\mu$ state, exactly cancels the integrated moment of the $+\mu$ subsystems below the line. The figure also shows the configuration of the plane in the presence of a negative holding field $-H_\mathrm{a} > -H_\mathrm{c}(0)$ and a *finite* thermal fluctuation field $H_\mathrm{T} = H_\mathrm{c}(0) - H_\mathrm{a}$. These two configurations differ in the orientation of the subsystems in the *shaded* region, which is $+\mu$ when $H_\mathrm{T} > 0$, compared with $-\mu$ when $H_\mathrm{T}=0$. Thus a thermal fluctuation field $H_\mathrm{T} > H_\mathrm{c}(0) - H_\mathrm{a}$ is necessary to reduce the moment to zero whenever $H_\mathrm{a} < H_\mathrm{c}(0)$. This "correction" becomes progressively more significant as $H_\mathrm{a} \to 0$, and leads to a progressively more severe upward deviation of the universal curve from linearity. When either $\sigma_\mathrm{d} \ll \bar{H}_\mathrm{d}$ or $\sigma_\mathrm{s} \ll \bar{H}_\mathrm{d}$, the shaded region is essentially unoccupied, and the deviation is negligible (except, of course, when $H_\mathrm{a}=0$ exactly, in which case $\ln t_\mathrm{c} \to \infty$ and hence $H_\mathrm{T} \to \infty$).

Similar comments apply to closely related analytical techniques,[5] which collapse the relaxation isotherms measured at the same temperature and over the same experimental time window, but in different holding fields, onto a common universal curve by the appropriate choice of a scaling variable. In the specific case of Ref. 5, this variable is the "athermal field" H_ath, which is defined as

$$H_\mathrm{ath}(t, H_\mathrm{a}, dH_\mathrm{a}/dt) = H_\mathrm{a} \pm H_\mathrm{f} \ln\left(\frac{t}{\tau_0} + \frac{H_\mathrm{f}}{\tau_0 |dH_\mathrm{a}/dt|}\right). \quad (8)$$

In the context of the current calculation, $H_\mathrm{a} \to -H_\mathrm{a}$, $\pm \to -$, and $|dH_\mathrm{a}/dt| \to \infty$, so that H_ath reduces to

$$H_\mathrm{ath} = -H_\mathrm{a} - H_\mathrm{f} \ln(t/\tau_0). \quad (9)$$

Figure 11 shows selected model relaxation isotherms from Fig. 6 replotted as a function of the modulus of the athermal

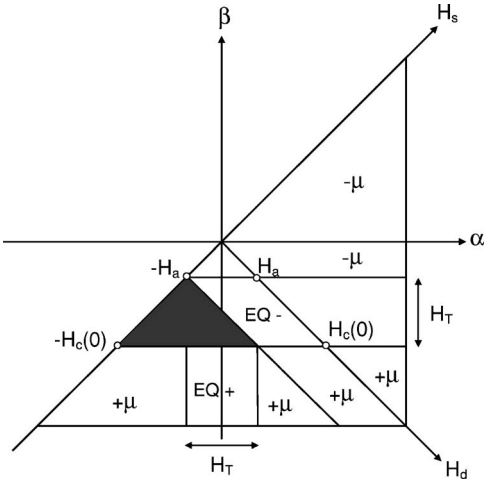

FIG. 10. The Preisach plane showing the origin of the deviation from linearity of universal curve in Fig. 7. The subsystems in the shaded region are in their $-\mu$ state when $H_T=0$, but remain in their $+\mu$ state in a negative holding field $-H_\mathrm{a} > -H_\mathrm{c}(0)$ and a thermal viscosity field $H_T = H_c(0) - H_\mathrm{a}$.

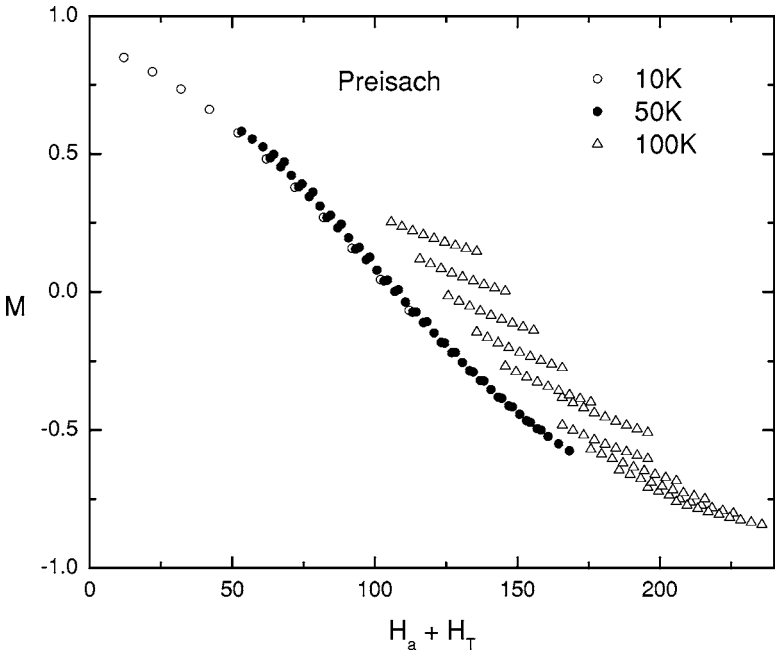

FIG. 11. Scaling plots of the relaxation isotherms in the three H_T windows in Fig. 6 as a function of the athermal field $|H_{\mathrm{ath}}|=H_{\mathrm{a}}+H_{\mathrm{T}}$. The different symbols distinguish numerical data from the three different temperatures $T=10$, 50, and 100 K.

field in Eq. (9). Isotherms from the three H_{T} windows bounded by the vertical lines in Fig. 6, corresponding to the same observation time interval 100 s$\leqslant t\leqslant 10^4$ s, but to three different temperatures $T=10$, 50, and 100 K, were plotted as a function of $|H_{\mathrm{ath}}|$ using the nominal model values for $H_{\mathrm{f}}=kT/\mu$ and τ_0. According to Fig. 11, this procedure yields good universal scaling behavior, with minimal dispersion, only at the very lowest measurement temperatures, with the dispersion becoming systematically more pronounced as the temperature increases. Moreover, the dispersion in the higher temperature windows can be improved significantly by treating H_{f} in Eq. (9) as an adjustable fitting parameter, and by decreasing H_{f} *below* its nominal model value $H_{\mathrm{f}}=kT/\mu$. Thus any attempt to extract the thermal fluctuation field from a superposition of viscosity isotherms will yield a maximum in H_{f} similar to that obtained from the analytical approach featured here.

[1] G. Bertotti, *Hysteresis in Magnetism* (Academic, New York, 1998).
[2] U. Atzimony, Z. Livne, R. D. McMichael, and L. H. Bennett, J. Appl. Phys. **79**, 5456 (1996).
[3] E. Della Torre and L. H. Bennett, IEEE Trans. Magn. **37**, 1118 (2001).
[4] E. Della Torre, L. H. Bennett, R. A. Fry, and O. A. Ducal, IEEE Trans. Magn. **38**, 3409 (2002).
[5] V. Basso, C. Beatrice, M. LoBue, P. Tiberto, and G. Bertotti, Phys. Rev. B **61**, 1278 (2000).
[6] L. Néel, Ann. Geophys. (C.N.R.S.) **5**, 99 (1949).
[7] S. Rao, E. Della Torre, L. H. Bennett, H. M. Seyoum, and R. E. Watson, J. Appl. Phys. **97**, 10N113 (2005).
[8] E. Della Torre, L. H. Bennett, and R. E. Watson, Phys. Rev. Lett. **94**, 147210 (2005).
[9] F. Preisach, Z. Phys. **94**, 277 (1935).
[10] L. Néel, J. Phys. Radium **11**, 49 (1950).
[11] J. Souletie, J. Phys. **44**, 1095 (1983).
[12] T. Song, R. M. Roshko, and E. D. Dahlberg, J. Phys.: Condens. Matter **13**, 3443 (2001).